Wake Interactions Between Groups of Undulating Foils

John Kelly¹, Yu Pan², and Haibo Dong³

University of Virginia, Charlottesville, VA, 22903, United States of America

The canonical motion of foils has been studied extensively in many applications, including energy harvesting. The advantage of undulating foils is often realized in their ability to positively interfere with neighboring foils. However, more research is needed in understanding different arrangements of undulating foils, along with the fluid dynamics interactions involved in enhancing the performance of the foils for this advantage to properly scale to a large number of foils. This work utilizes the concept of subgroups within a school, borrowed from biological studies of fish schools, along with an immersed boundary method-based computational fluids solver to investigate how these larger groups of undulating foils interact. A parametric study is completed around the spacing of the back subgroup, and the vortex formation and wake structures are analyzed, revealing that the back subgroup gains efficiency via interactions with the wake of the front subgroup. The present study gives insight into how groups of undulating foils interact and uncovers mechanisms that enhance performance through their interaction.

I. Nomenclature

T period of motion λ wavelength of the motion Re Reynolds number p hydrodynamic pressure cfoil chord length ν kinematic viscosity freestream velocity tail motion amplitude Atail beat frequency Strouhal number fluid density C_T = thrust coefficient C_{Pw} power coefficient = x force coefficient = Froude efficiency

= z - vorticity

 ω_z

II. Introduction

Harvesting energy from the environment has received increasing attention in both renewable energy and robotics fields. Wind turbines have been shown to have both positive and negative interference, and even show the potential to harvest more energy by gaining energy from the vortices shed by neighboring turbines. Engineers have increasingly looked to examples provided in nature for improving engineering designs. In an effort to improve the interaction

¹ Ph.D. Student, Mechanical and Aerospace Engineering, AIAA Student Member

² Ph.D. Student, Mechanical and Aerospace Engineering, AIAA Student Member

³Professor, Mechanical and Aerospace Engineering, AIAA Associate Fellow

between wind turbines, Whittlesey et al. used a potential flow model along with experimental measurements to show that the wake structures of fish swimming and vertical axis wind turbines (VAWT) are very similar [1]. This study shows that arranging VAWT's in a fish-school-like formation can lead to better energy output from the turbines. In addition, many other studies have shown that energy harvesting can be accomplished via multiple foils in a staggered formation [2]. To optimize the energy harvested by multiple foil systems further, the fluid dynamics of a large number of foils must be understood. The current fluid studies in both energy harvesters and fish schooling rely on significantly simplified models or very few total bodies. To better understand how to position a large number of energy harvesters to optimize energy output, more research is needed in fish-school-like formations.

Previously, the study of complex flow interaction in unsteady multi-body fluid simulations is typically done using similar geometric simplifications and prescribed motion models. [3] These studies include many examples utilizing two bodies, including studying the stability of two-foil systems [4] and utilizing reinforcement learning controlling arrangements to optimize performance in a two-foil system [5]. Moving to a larger number of bodies, Pan and Dong previously studied four undulating foil arrangements, uncovering the wall effect and the block effect as the primary performance-enhancing interactions, along with the dense school as an optimum for a basic diamond arrangement [6-8].

Many biologists have also studied the arrangement of fish within a school to determine if questions about optimal school arrangements can be answered by the examples found in nature. In this work, they have uncovered that fish in a larger school tend to act as smaller subgroups, behaving and moving similarly to the fish within their subgroup but often varying across the larger school as a whole [9-11]. In this paper, research will be presented on undulating foil groups using this subgroup model found in biology utilizing computational fluids simulations to study the performance and underlying fluid dynamics. To generate the subgroups, the dense diamond four foil school shown to have a high performance by Pan et al. [6] is utilized as the basic subgroup shape. Next, a parametric study of in-line subgroups is shown, including changing the spacing between the subgroups and the width of the second subgroup. Finally, an analysis of the fluid interaction between subgroups and their effect on performance is shown.

III. Methods

A. Problem Definition

In keeping with typical two-dimensional fish swimming studies, the standard NACA0012 foil shape will be utilized as a baseline shape for fish-like Carangiform swimmers [6-8]. Traveling wave kinematics are imposed on the foil to give carangiform undulatory motion. The motion follows the equation:

$$y(x,t) = A(x) \cdot \sin\left(\frac{2\pi}{\lambda}x - \frac{2\pi}{T}t\right),\tag{1}$$

where x and y are normalized by the body length of the foil, giving the head of the fish at x=0 and the tail at x=1. The value of y(x,t) corresponds to the lateral deviation of the body of the foil from the original foil chord. T is the period of the traveling wave, and λ is the wavelength of the wave. A(x) denotes the amplitude of the lateral motion and is expressed as a quadratic polynomial given by:

$$A(x) = a_2 x^2 + a_1 x + a_0, (2)$$

where the coefficient values are chosen to be $a_2 = 0.02$, $a_1 = -.08$, and $a_0 = 0.16$, matching the previous study completed by Pan et al. [6]. The resulting motion can be seen in Fig. 1a.

The base subgroup shape of a four-foil dense diamond is shown in Fig. 1b, where c is the chord length, S is the streamwise spacing, G is the streamwise gap between groups, and D is the lateral spacing. In keeping consistent with the previous work of Pan et al. [6], we use a c value of 1, an S value of 0.4, and D and G values of 0.4 initially. In this study, both G and D are varied in the second subgroup, along with changing the orientation of the second subgroup.

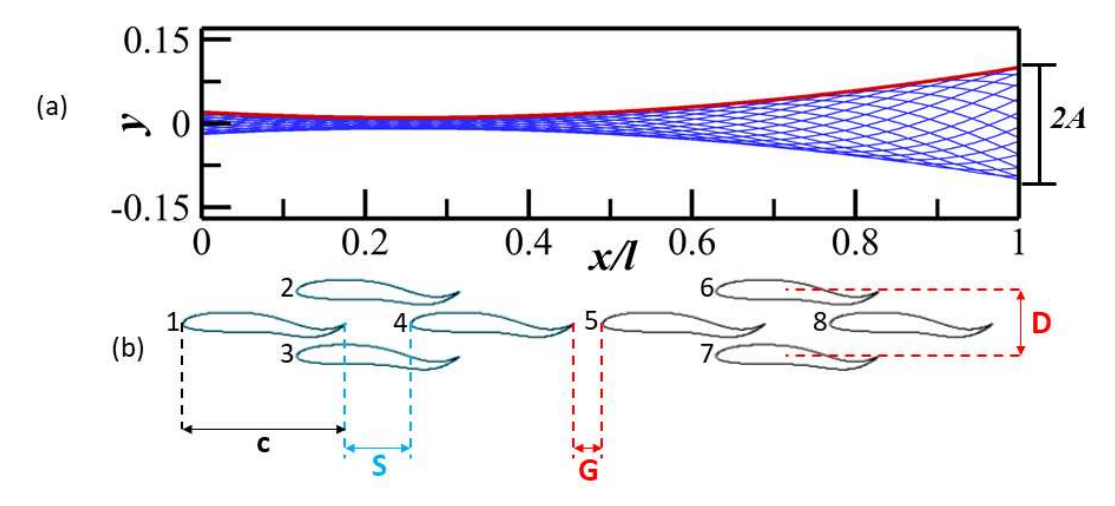


Fig. 1 (a) Traveling wave amplitude (red) and the midlines of the body motion (blue) for a single tail beat period. (b) Arrangement definitions for front (blue) and back (black) subgroups: foil length (c), streamwise spacing the (S), streamwise gap between subgroups (G), and lateral spacing (D). The individual foils are also labeled.

B. Numerical Methods

The two-dimensional incompressible Navier-Stokes equations govern the flow in the numerical solver used and are written in index form and expressed in their nondimensional form as:

$$\frac{\partial u_i}{\partial x_i} = 0, (3)$$

$$\frac{\partial u_i}{\partial x_i} = 0,$$

$$\frac{\partial u_i}{\partial t} + \frac{\partial u_i u_j}{\partial x_j} = -\frac{\partial p}{\partial x_i} + \frac{1}{Re} \frac{\partial^2 u_i}{\partial x_i \partial x_j},$$
(4)

where the z terms are all zero, u_i are the velocity components, p is the pressure, and Re is the Reynolds number. The equations are discretized using a cell-centered, collocated arrangement of the primitive variables and is solved using a finite difference-based Cartesian grid immersed boundary method. The solver has been successfully implemented previously in canonical cases [12-14], as well as biological flying [15-17] and swimming [18-19], and has been validated extensively. More information about the solver can be found in [20-21]. To understand our results, we first use the force coefficient in the x direction:

$$C_x = F_x/(0.5\rho U_\infty^2 c^2),$$
 (5)

where F_x is the instantaneous net force in the x direction, ρ is the fluid density, U_{∞} is free stream velocity and c is the foil chord length. We then averaged C_x over one period of motion for each foil, giving $\overline{C_x}$, corresponding to the net force in the x direction over a cycle of motion. Similarly, the coefficients of thrust and power can be computed as:

$$C_T = F_T/(0.5\rho U_{\infty}^2 c^2),$$
 (6)

$$C_{PW} = Pw/(0.5\rho U_{\infty}^3 c^2),$$
 (7)

where F_T is the instantaneous thrust and Pw is the instantaneous power consumed for the undulating motion. The averages over a period of motion are also computed, giving the results of $\overline{C_T}$, which is the net thrust over a cycle of motion, and $\overline{C_{Pw}}$, which is the net power consumed over a cycle of motion. Finally, the efficiency is calculated using a modified form of the Froude efficiency, which is defined as a ratio of useful power to total power:

$$\eta = \frac{\overline{C_T}}{\overline{C_T} + \overline{C_{Pw}}} \tag{8}$$

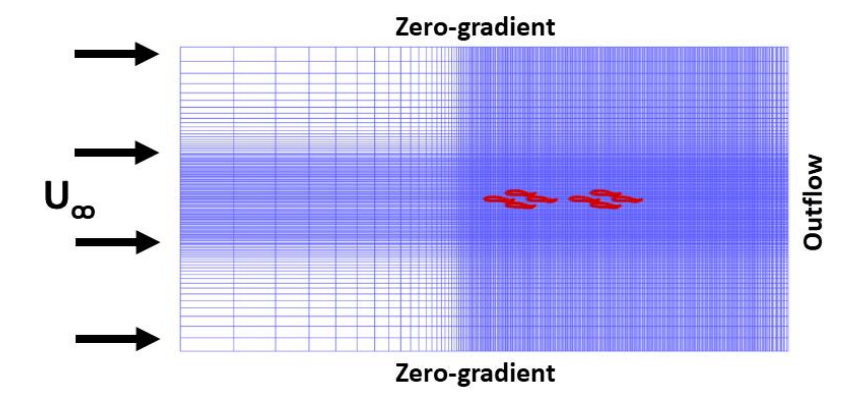


Fig. 2 Representative cartesian grid and boundary conditions with baseline subgroup arrangement

The flow simulation is set up with the computational grid and boundary conditions shown in Fig. 2. For this study, the flow conditions are described by two dimensionless parameters, the Reynolds number (Re) and the Strouhal number (St), defined as:

$$Re = \frac{U_{\infty c}}{v}, \tag{9}$$

$$Re = \frac{U_{\infty c}}{v},$$

$$St = \frac{2fA}{U_{\infty}},$$
(9)

where v is the kinematic viscosity of the fluid, f is the tail beat frequency and A is the amplitude of the lateral motion at the tail tip. The Reynolds number is chosen to be 1,000 to mimic fish swimming. The Strouhal number is chosen to keep the cases near the free-swimming condition, where $\overline{C_x}$ is near zero, based on the single undulating foil case. This results in a Strouhal number of 0.42.

IV. Results

A. Performance of Single and In-Line Groups

First, the baseline case is compared to the single 4-foil narrow diamond school. The values for the cycle average C_x and η are given in Table 1. The table includes the average over all 4 of the four-foil school, all 8 foils of the in-line groups, and the averages for each subgroup. The primary conclusion from these results is that there is a significant average performance enhancement in both C_x and η when going from a single subgroup to two subgroups. We also see that the primary enhancement in Cx comes from enhancement in the front subgroup, whereas the back subgroup sees the largest enhancement in efficiency.

Average	4 Foil School	In-Line Subgroups	Front Subgroup	Back Subgroup
$\overline{C_x}$	0.058	0.065	0.075	0.055
η	0.535	0.552	0.542 (+1.3%)	0.561 (+4.9%)

Table 1 Cycle averaged values for each group and subgroup in the baseline configuration

Next, the vorticity and x-velocity averages are shown in Fig. 3. In comparing the vorticity for the single 4-foil school to the in-line subgroups (a,b), we see a very similar wake structure with a 2S center wake and a 2P wake on the edges. In part (b), we note that the vortices shed by the front subgroup are not entirely captured by the back subgroup, giving evidence that a wider back subgroup may be able to better utilize the energy from the vortices shed by the front subgroup. Additionally, we see that the wake structure is much more symmetric and coherent for the 4-foil school, giving more distinct jets in the velocity average plots.

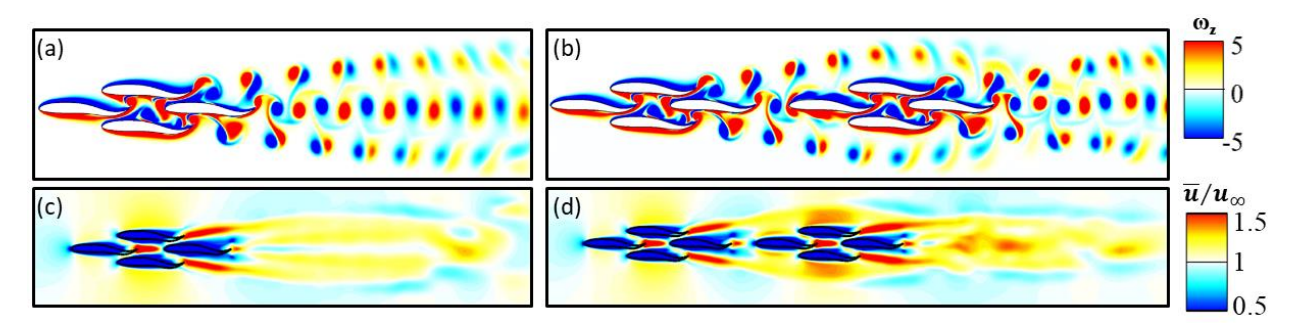


Fig. 3 Vorticity (a,b) and velocity average (c,d) plots for the 4 foil school (a,c) and in-line subgroups (b,d)

B. Efficiency Increase in the Back Subgroup via Vortex Interactions

Next, the spacing between subgroups (G) is varied, along with the lateral spacing of the back subgroup (D) to manipulate the interaction with the front school wake and fully capture the wider spacing of the front subgroup's 2P vortex pairs. The resulting efficiency averaged over the second subgroup, η_{Back}^* , is shown in Fig. 4.

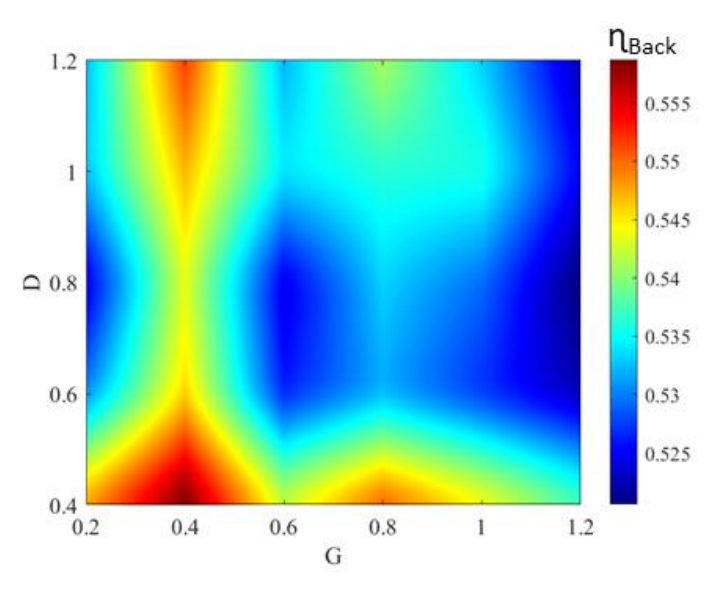


Fig. 4 Average efficiency in the back subgroup for changes in spacing between subgroups (G) and lateral spacing in the second subgroup (D).

First, it is seen that both D and G have a significant impact on the efficiency in the second subgroup, with a range of 8% in the efficiency occurring from small changes in the spacing. The highest efficiency occurs when both G and D are 0.4. The densest spacing provides the most beneficial interaction within a dense school, via the wall, block, and body-body suction effects detailed by Pan and Dong, and the spacing is consistent with the most beneficial found in their study [6-7]. The next highest efficiency zones, however, occur at the maximum D value, where it is expected that the beneficial dense school interactions are at a minimum within the back subgroup. Additionally, there is another pair of higher efficiency zones at G = 0.8 at the lowest and highest D values, creating another vertical band of increased performance.

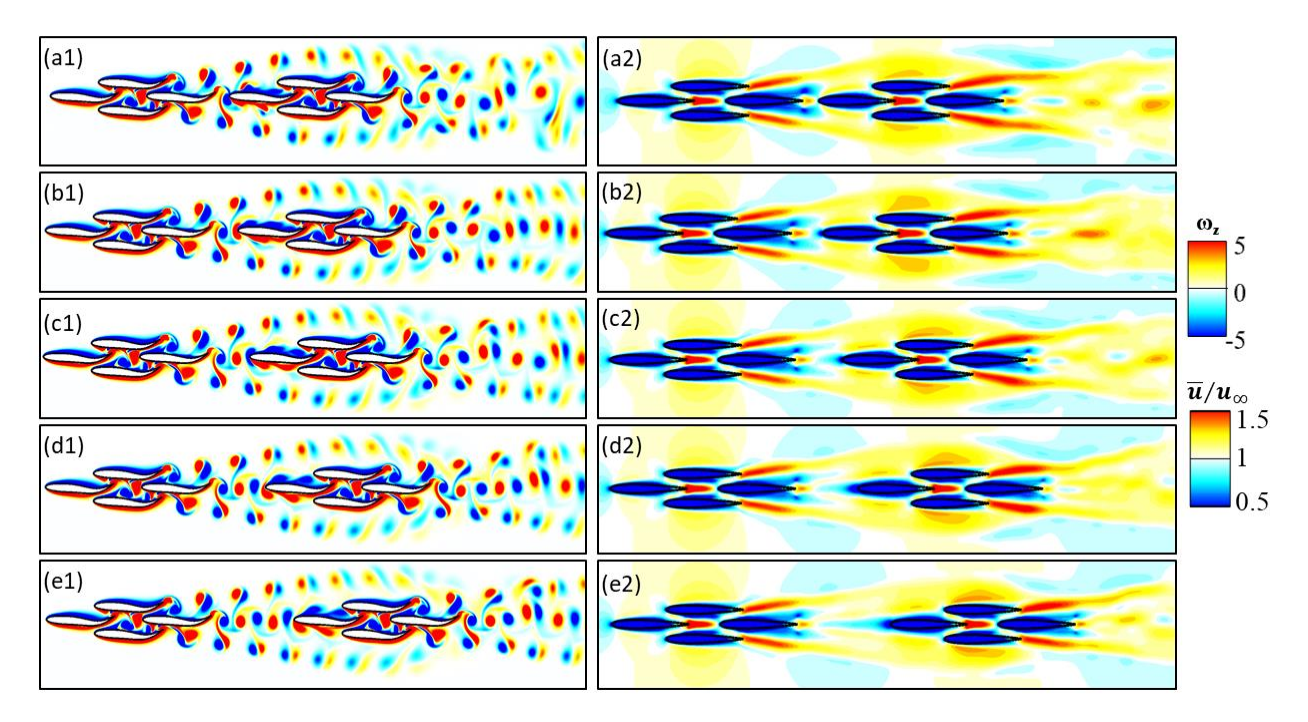


Fig. 5 Vorticity (1) and cycle-average streamwise velocity (2) for G = 0.2 (a), 0.4 (b), 0.6 (c), 0.8 (d), and 1.2 (e) at D = 0.4.

The vorticity for G = 0.2, 0.4, 0.6, 0.8, and 1.2 along D = 0.4 is shown in Fig. 5, including the efficiency peaks at 0.4 and 0.8, and the lower performing cases between. Across all of the cases, the typical 2S core and 2P vortex pairs are observed in the wake, corresponding to short jets on the edge of the school in the velocity average. The primary difference in the near-body vortices with the change in G is observed along the leading-edge vortex of foil 5. As the 2S wake core from foil 4 intersects with the body of foil 5, there is constructive and destructive interference with the leading-edge vortex depending on the spacing. In the highest performing cases (b1, d1), there is primarily constructive interaction and subsequent enhancement in the leading-edge vortex of foil 5 from the wake of foil 4. With the lower-efficiency spacing, there are significant amounts of destructive interaction and interruption of the leading-edge vortex along the body of the foil. The effect of this can be seen in Fig. 6, which shows the net force and power consumption over a cycle of motion for G = 0.4 and G = 0.6 at D = 0.4 in foil 5. In the figure, both the thrust enhancement and power reduction are seen, particularly at t/T = 0.25 and 0.35 respectively, along with t/T = 0.75 and 0.85 due to symmetry.

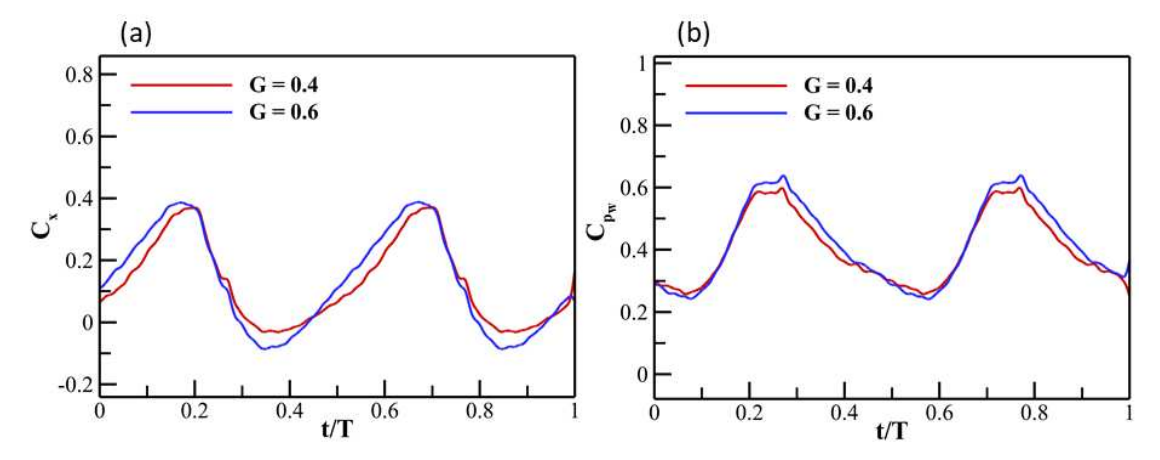


Fig. 6 Coefficient of force (a) and power (b) for G = 0.4 and 0.6 at D = 0.4.

The performance benefit due to this interaction occurs because the wake from foil 4 is repeated, such that the oncoming vortices are similar by moving the second subgroup back by the distance between two of the same sign vortices in the wake. For these parameters, this corresponds to a spacing of 0.46l. The vertical bands in Fig. 4 are attributed to this, and the spacing of 0.4l in the figure is very close to the 0.46l attributed to the wake. Should the study continue to G = 1.4 and beyond, it is predicted that the pattern repeat as the constructive wake interaction continues. Streamwise spatial changes resulting in a banded structure in the efficiency from similar interactions with a repeating wake has been also been observed in the interaction of 2 foils, as presented in Boschitsch et al. [22].

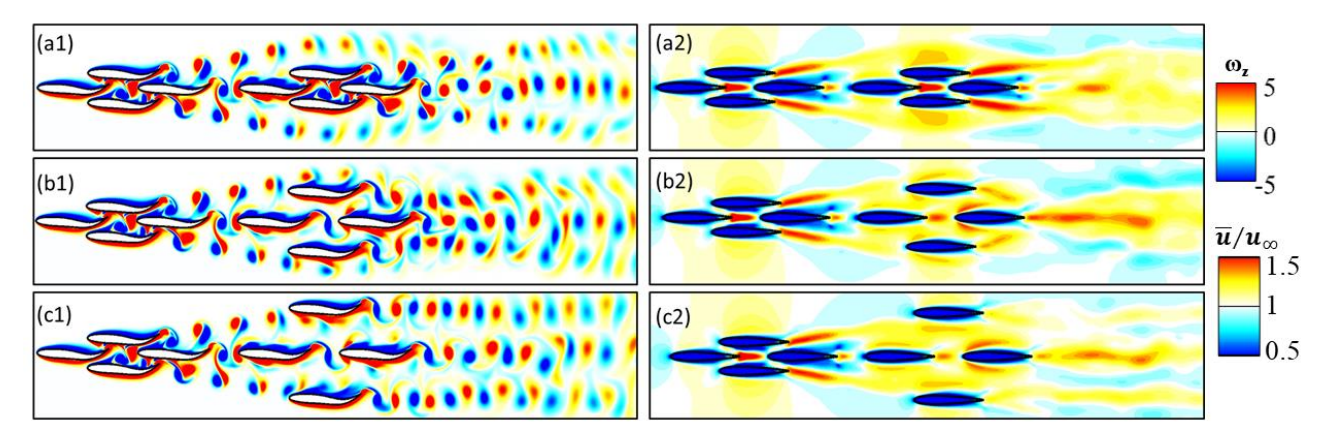


Fig. 7 Vorticity (1) and cycle-average streamwise velocity (2) for D = 0.4 (a), 0.8 (b), 1.2 (c) at G = 0.4.

Next, the vorticity is shown for D = 0.4, 0.8, and 1.2 at G = 0.4 in Fig. 7. At D = 0.4, the wake behind the second subgroup has the same structure as the diamond school, with a 2S core and 2P pairs of vortices on either side. The school intersects the 2S pair from foil 4, while completely missing the 2P pairs which move laterally around the subgroup. In the medium width D = 0.8, the 2P pairs from the front school are partially captured by the outer foils in the second subgroup. The vortices destructively interfere with the leading-edge vortex of that foil. The resulting wake begins with a 2S pair behind each of the outer foils, but transitions to a 2P pair farther downstream. At D = 1.2, the 2P wake pair from the front subgroup are captured on the inside of the outer foils. This creates constructive interference with the leading-edge vortex. The resulting wake is wider, with 3 sets of 2S pairs. The effects of the vortex interactions can be seen in Fig. 8, which details the net force and power consumption in foil 6 over a cycle of motion. In the figure, the higher power consumption and net force resulting from denser schooling interactions are seen at D = 0.4, whereas D = 0.8 and D = 1.2 have more consistent results with smaller peaks and troughs and are lower in both power consumed and net thrust generated. The main difference between the latter two occurs when the foil is flapping outward from the school. The leading-edge vortex enhancement gives both a power and a thrust benefit to D = 1.2.

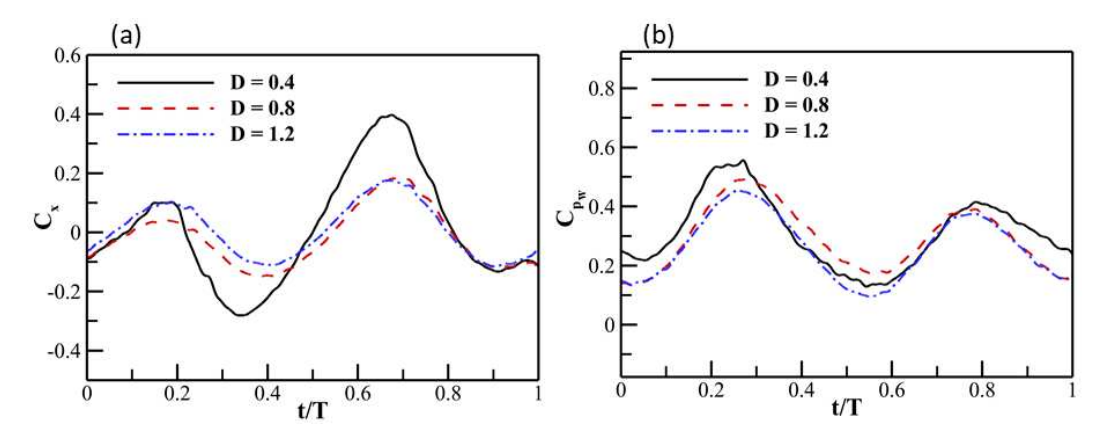


Fig. 8 Coefficient of force (a) and power (b) for D = 0.4, 0.8, and 1.2 at G = 0.4.

C. Thrust Enhancement in the Front Subgroup via Increased Pressure

Next, to discuss the net force enhancement in the front subgroup, the average of the subgroup net force over a cycle of motion is shown for changes in G and D in Fig. 9. In the figure, the highest net force is achieved for the smallest G values, and the effect is almost entirely independent of D. As the subgroups get closer, the thrust in the front subgroup is increased, dropping off quickly as the schools become farther apart to almost the single diamond school value of 0.06.

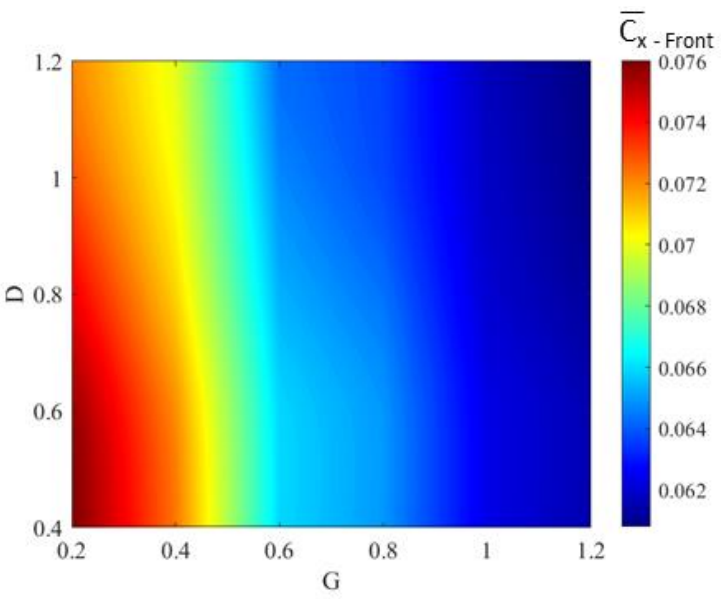


Fig. 9 Average net force in the front subgroup for changes in spacing between subgroups (G) and lateral spacing in the second subgroup (D).

The cycle averaged pressure at G = 0.2 and G = 0.4 are shown in Fig. 10. In the figure, a low-pressure zone exists between the schools in the G = 0.4 case, but not at G = 0.2. The low pressure provides suction at the back of foil 4, providing some drag to the foil and preventing a higher thrust to be generated by the back of the foil. In the closer case, there is less of a low-pressure zone, so there is less suction and more thrust generation on foil 4. Similar effects have been reported in [22-23], showing that in a two-body system at very small streamwise spacing, drag reduction and thrust enhancement result from an increase in the pressure between the bodies. These results are also very similar to the block effect previously reported in dense diamond fish schools [6]. The results indicate that a similar thrust enhancement occurs between subgroups within a larger school with small streamwise spacing between the subgroups.

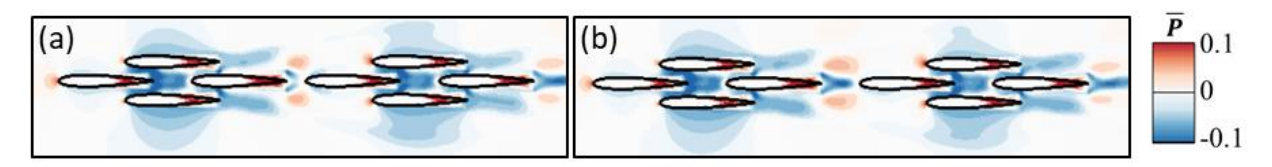


Fig. 10 Cycle average pressure contour for G = 0.2 (a) and G = 0.4 (b) at D = 0.4.

V. Conclusions

Two-dimensional numerical simulations have been conducted to study the interaction between 2 subgroups of undulating foils in dense diamond formations. It is shown that the addition of a second diamond subgroup enhances the performance of both subgroups, with the back subgroup primarily gaining efficiency while the front subgroup primarily increases in the net force. The wake structures within the two-subgroup system are identified, and two primary vortex capture mechanisms are identified for enhancing the efficiency in the second subgroup. First, changing the spacing between the subgroups showed enhancement of the leading-edge vortex via constructive interference with the center wake of the front subgroup led to better performance in the back subgroup. This creates a repeating high-efficiency zone based on the spacing of the subgroups. Second, high efficiency in the second subgroup can be achieved

either by swimming compactly to maximize the interaction within the subgroup or in a wider formation to fully capture the wake of the front subgroup such that the leading-edge vortex of the outside pair are enhanced by the wake interaction. The improvement in performance for the front subgroup was shown to occur due to the thrust increase that results from the proximity of the two subgroups, and the advantage dissipates as the spacing between subgroups increases. Overall, the efficiency gain in the second subgroup is shown to be heavily dependent on both the lateral spacing of the subgroup and the space between groups. This ranges from 8% efficiency gains in the subgroup to a negative effect on efficiency from swimming in a subgroup in the worst cases. The net force benefit in the front subgroup was shown to rely solely on the spacing between the subgroups, benefitting most when they are the closest together.

Acknowledgments

This work was supported by ONR MURI N0014-14-1-0533, ONR MURI N00014-15-1-2234, and NSF CNS - 1931929. Additionally, thanks to the University of Virginia Research Computing Group for the availability of the Rivanna supercomputing cluster.

References

- [1] Whittlesey, Robert W., Sebastian Liska, and John O. Dabiri. "Fish Schooling as a Basis for Vertical Axis Wind Turbine Farm Design." Bioinspiration and Biomimetics 5, no. 3 (2010). https://doi.org/10.1088/1748-3182/5/3/035005.
- [2] Xu, Wenhua, Guodong Xu, Wenyang Duan, Zhijie Song, and Jie Lei. "Experimental and Numerical Study of a Hydrokinetic Turbine Based on Tandem Flapping Hydrofoils." Energy 174 (2019): 375–85. https://doi.org/10.1016/j.energy.2019.02.188.
- [3] Khalid, M. S. U., Akhtar, I., & Dong, H. (2016). Hydrodynamics of a tandem fish school with asynchronous undulation of individuals. Journal of Fluids and Structures, 66, 19–35. https://doi.org/10.1016/j.jfluidstructs.2016.07.008
- [4] Kurt, Melike, Pedro Costa, Amin Mivehchi, and Keith W. Moored. "Two-Dimensionally Stable Self-Organization Arises in Simple Schooling Swimmers through Hydrodynamic Interactions." Preprint, no. February (2021).
- [5] Novati, Guido, Siddhartha Verma, Dmitry Alexeev, Diego Rossinelli, Wim M. Van Rees, and Petros Koumoutsakos. "Synchronisation through Learning for Two Self-Propelled Swimmers." Bioinspiration and Biomimetics 12, no. 3 (2017). https://doi.org/10.1088/1748-3190/aa6311.
- [6] Pan, Yu, and Haibo Dong. "Computational Analysis of Hydrodynamic Interactions in a High-Density Fish School." Physics of Fluids 32, no. 12 (2020). https://doi.org/10.1063/5.0028682.
- [7] Pan, Y., Han, P., Huang, J., & Dong, H. (2020). Effect of Formation Pattern on Schooling Energetics in Fish-Like Swimming FEDSM2020, 1–8.
- [8] Pan, Y., & Dong, H. (2022). Effects of phase difference on hydrodynamic interactions and wake patterns in high-density fish schools. Physics of Fluids, 34(111902), 1–25. https://doi.org/10.1063/5.0113826.
- [9] Reuter, Hauke, and Broder Breckling. "Selforganization of Fish Schools: An Object-Oriented Model." Ecological Modelling 75–76, no. C (1994): 147–59. https://doi.org/10.1016/0304-3800(94)90014-0.
- [10] Chang, Xinfeng, Zhongqiang Pan, and Limin Luo. "Community Detection Based on Fish School Effect." IEEE Access 10 (2022): 48523–38. https://doi.org/10.1109/ACCESS.2022.3172298.
- [11] Partridge, Brian L. "Internal dynamics and the interrelations of fish in schools." J. Comp. Physiol. 144, 313-325 (1981). https://doi.org/10.1007/BF00612563
- [12] Narasimhan, M., Dong, H., Mittal, R., & Singh, S. N. (2006). Optimal yaw regulation and trajectory control of biorobotic AUV using mechanical fins based on CFD parametrization. Journal of Fluids Engineering, Transactions of the ASME, 128(4), 687–698. https://doi.org/10.1115/1.2201634
- [13] Kelly, J., Han, P., Dong, H., & Van Buren, T. (2021). Wake Structures and Effect of Hydrofoil Shapes in Efficient Flapping Propulsion. FEDSM2021, 1–7.
- [14] Kelly, J., Pan, Y., & Dong, H. (2022). Body Shape Effects on the Hydrodynamic Performance of Bio-Inspired Undulating Swimmers. FEDSM2022, 1–6. https://doi.org/10.1115/FEDSM2022-87645
- [15] Li, C., Dong, H., & Zhao, K. (2018). A balance between aerodynamic and olfactory performance during flight in Drosophila. Nature Communications, 9(1), 1–8. https://doi.org/10.1038/s41467-018-05708-1
- [16] Ren, Y., Dong, H., Deng, X., & Tobalske, B. (2016). Turning on a dime: Asymmetric vortex formation in hummingbird maneuvering flight. Physical Review Fluids, 1(5), 2–4. https://doi.org/10.1103/physrevfluids.1.050511
- [17] Bode-Oke, A. T., Zeyghami, S., & Dong, H. (2017). Aerodynamics and flow features of a damselfly in takeoff flight. Bioinspiration and Biomimetics, 12(5). https://doi.org/10.1088/1748-3190/aa7f52
- [18] Lauder, G. V., Madden, P., Hunter, I., Tangorra, J. L., Davidson, N., Proctor, L., Mittal, R., Dong, H., & Bozkurttas, M. (2005). Design and performance of a fish fin-like propulsor for AUVs. Proceedings of 14th International Symposium on Unmanned Untethered Submersible Technology (UUST), 1–13.
- [19] Pan, Y., Zhang, W., & Dong, H. (2022, August). Computational Modeling and Hydrodynamic Analysis of Fish Schools in Three-Dimensional Arrangements. FEDSM2022 (Vol. 85840, p. V002T05A024). American Society of Mechanical Engineers.

- [20] Bozkurttas, M., H. Dong, V. Seshadri, R. Mittal, and F. Najjar. "Towards Numerical Simulation of Flapping Foils on Fixed Cartesian Grids." 43rd AIAA Aerospace Sciences Meeting and Exhibit - Meeting Papers, no. December 2014 (2005): 15801– 9. https://doi.org/10.2514/6.2005-79.
- [21] Zhang, W., Pan, Y., Wang, J., Di Santo, V., Lauder, G. V., & Dong, H. An Efficient Tree-Topological Local Mesh Refinement on Cartesian Grids for Multiple Moving Objects in Incompressible Flow. SSRN 4169528.
- [22] Boschitsch, B. M., Dewey, P. A., & Smits, A. J. (2014). Propulsive performance of unsteady tandem hydrofoils in an in-line configuration. Physics of Fluids, 26(5). https://doi.org/10.1063/1.4872308 [5] Pan, Yu, and Haibo Dong. "Computational Analysis of Hydrodynamic Interactions in a High-Density Fish School." Physics of Fluids 32, no. 12 (2020). https://doi.org/10.1063/5.0028682.
- [23] Ristroph, L., & Zhang, J. (2008). Anomalous hydrodynamic drafting of interacting flapping flags. Physical Review Letters, 101(19), 1–4. https://doi.org/10.1103/PhysRevLett.101.194502